UAV Aircraft Carrier Landing Using CFD-Based Model Predictive Control

Joseph Lorenzetti*, Andrew McClellan†, Charbel Farhat‡, and Marco Pavone§
Stanford University, Stanford, CA, 94305

The control problem associated with autonomous aircraft carrier landings for UAVs is challenging due to requirements on safety, high-performance operation, and uncertain and highly dynamic environments. This work proposes a control scheme for such problems that enables safe operation of the UAV at the limits of its performance by utilizing a model predictive control (MPC) approach. While real-time computation requirements typically limit the fidelity of the models used in optimization-based control, in this work it is demonstrated that high-fidelity computational fluid dynamics (CFD) models can be used within an MPC framework via the construction of a projection-based reduced order model (ROM). An application of a CFD-based MPC scheme to the glideslope tracking problem is then developed to demonstrate the effectiveness of the proposed approach.

I. Introduction

As the technology surrounding Unmanned Aerial Vehicles (UAVs) has developed, the tasks that they are expected to perform have become increasingly complex. One such task, recognized for its importance by the US Department of Defense [1], is fully autonomous carrier landing. Automation systems currently in use, such as the Automatic Carrier Landing System (ACLS) and the Precision Approach and Landing System (PALS) [2, 3], still require significant human supervision or action, can only operate in nominal conditions, and are tailored to piloted aircraft. Approaches that have been proposed for fully autonomous carrier landings have utilized robust linear control methods [4, 5], adaptive control, fuzzy logic, neural networks [6], dynamic inversion [6, 7], linear quadratic gain-scheduling [8], and model reference adaptive control [9]. While these methods find success for nominal landing scenarios, they do not satisfactorily address situations requiring high performance control, constraint handling, time-varying objectives, and autonomous abort decision making. Enabling *safe* and *fully autonomous* landings requires that the control scheme account for such situations, for example to land in high sea states, recover from bolters (unarrested landings), handle wave-offs, and minimize dispersions and sink rates prior to landing. To address these complex considerations we propose the use of a model predictive control (MPC) scheme.

Model predictive control [10] is a flexible, model-based control approach that can explicitly handle state and control constraints while optimizing performance. For the autonomous carrier landing problem, the inclusion of state and control constraints in MPC provides an important advantage over existing techniques. Specifically, it allows the UAV to safely operate at its *performance limits*, and provides an implicit capability to make autonomous abort decisions when constraint violation is unavoidable. From a performance standpoint, the MPC cost function provides a flexible avenue for handling time-varying mission objectives. For example during the initial descent phase the deviation from a nominal glideslope trajectory could be minimized, and then upon final approach the objective could be switched to a more landing-specific performance metric such as landing dispersion or sink rate.

Model predictive control has already been shown to be an effective control scheme for aerospace applications [11]. Of particular interest are previous works that have applied MPC-based control schemes to the autonomous carrier landing problem. The approach in [12] addresses the glideslope tracking problem (i.e. tracking a nominal approach to the carrier) by designing an MPC controller based on a linearized longitudinal aircraft dynamics model and a linear carrier motion model, but does not consider the effect of disturbances. Then, in [13] a stochastic MPC scheme is proposed which focuses on glideslope tracking in the presence of uncertain wind gusts, described by a Dryden turbulence model. This work was then extended in [14] to consider measurement uncertainty, a carrier airwake model, and a carrier

*Ph.D. Candidate, Department of Aeronautics and Astronautics, William F. Durand Building, jlorenze@stanford.edu.
†Ph.D. Candidate, Department of Aeronautics and Astronautics, William F. Durand Building, amcclell@stanford.edu.
‡Vivian Church Hoff Professor of Aircraft Structures, Department of Aeronautics and Astronautics, Department of Mechanical Engineering, and Institute for Computational and Mathematical Engineering, William F. Durand Building, cfarhat@stanford.edu. Fellow AIAA.
§Associate Professor, Department of Aeronautics and Astronautics, William F. Durand Building, pavone@stanford.edu.

motion model. A dynamics model with slightly higher fidelity is used in [15], which addresses a helicopter ship-based landing problem. Specifically, the helicopter model incorporates dynamics from rigid-body motion, a simplified rotor blade structural model, and a simplified rotor aerodynamics model. Additionally, a carrier airwake model built from computational fluid dynamics (CFD) data is included, but only by interpolation with piecewise polynomial functions. In these approaches [12–15] the inclusion of models beyond the nominal aircraft rigid-body dynamics reflects the fact that MPC control in such a high performance environment requires models with increased sophistication. Yet the computational requirements of MPC have still limited these approaches to relatively simple models. This work seeks to overcome some of these challenges by leveraging both the modeling power of computational fluid dynamics techniques and the efficiency gained from reduced order modeling. Specifically, we demonstrate the use of a CFD-based reduced order aerodynamics model within an MPC control scheme. This extends previous approaches by showing that principled, high-fidelity models generated from CFD methods can be used for model-based aircraft control.

Model order reduction techniques [16], such as balanced truncation or proper orthogonal decomposition (POD), are principled methods for generating approximate dynamics models of reduced order from potentially very high-dimensional systems (e.g. arising from discrete approximations to infinite-dimensional systems). In particular, CFD-based reduced order models (ROMs) have been successfully used for tasks such as simulation, optimization, and control. For example [17] uses a CFD-based aeroelastic ROM to include flutter constraints for an aircraft trajectory optimization problem solved through dynamic programming. Also, similar to our proposed approach, a CFD-based MPC controller is used in [18] for shock position control in a supersonic jet engine inlet. However this work assumes full state observability, the stability and robustness of the control scheme are not discussed, and only soft constraints are imposed so as to ensure persistent feasibility of the MPC algorithm. In this work, we leverage recent advances in reduced order model predictive control (ROMPC) [19, 20] to design a CFD-based MPC scheme that can track a nominal glideslope, has guarantees on robust constraint satisfaction and stability, and incorporates a state observer.

Contributions: In this work we show that high-fidelity CFD models describing the aerodynamics of a UAV can be utilized within a model predictive control scheme via the construction of reduced order models. A CFD-based MPC scheme for glideslope trajectory tracking is then designed using a reduced order CFD model generated via balanced truncation with dimension $n_{\text{ROM}} = 20$ where the original CFD model had $n_{\text{CFD}} = 10,410$ degrees of freedom, and the effectiveness of the controller is demonstrated in simulation. In addition, guarantees are provided on robust state and control constraint satisfaction of the UAV system in the presence of state estimation error, bounded disturbances, *and* model reduction error.

Organization: In Section II we begin by describing at a high level the objectives associated with the controller design and some relevant assumptions made about the system. The description of the system dynamics begins with the definition of relevant reference frames in Section II.A and then continues in Section III where the linearized aerodynamics and rigid-body models are described in detail. The resulting combined rigid-body/fluid system model, referred to as the full order model, is then given in Section III.D and is followed by the definition of the reduced order model in Section III.E. In Section IV the CFD-based MPC scheme is described, including the reduced order MPC problem, the reduced order state estimator, and the UAV control law. Finally, in Section V we demonstrate the ability of the proposed control scheme to drive a UAV to track a glideslope trajectory in simulation.

II. Problem Formulation

The problem considered in this work is to design a control scheme that allows a UAV to track a predefined glideslope trajectory during the approach phase of a carrier landing. We restrict our attention to longitudinal plane motion and define the nominal glideslope trajectory (fixed relative to Earth) by a flight path angle γ_0 and a constant desired UAV velocity V_0. We assume the aircraft operates under constraints on its physical state (e.g. angle-of-attack, distance from glideslope) and with limited control authority (e.g. limited thrust), and that we have access to measurements of position, velocity, pitch angle, and pitch rate. Additionally, it is assumed that the available measurements may be corrupted by bounded noise and that unknown but bounded disturbances (e.g. wind) may influence the system dynamics.

A. Reference Frames

Using a flat-earth assumption, we define a series of coordinate systems: (1) an Earth-fixed inertial frame $\mathcal{I}$, (2) a body-fixed frame $\mathcal{B}$, aligned with the principal axes of the aircraft, and (3) an (inertial) relative frame $\mathcal{R}$ that moves along the glideslope at the constant velocity V_0 and with a constant angular offset θ_0 from $\mathcal{I}$. The relationship between $\mathcal{I}$ and $\mathcal{R}$ is given in Figure 2, where the glideslope is defined by the flight path angle γ_0, and α_0 is the equilibrium angle of attack for the UAV. In the definition of the angles in Figure 2, arrows indicate direction of increasing angle and an

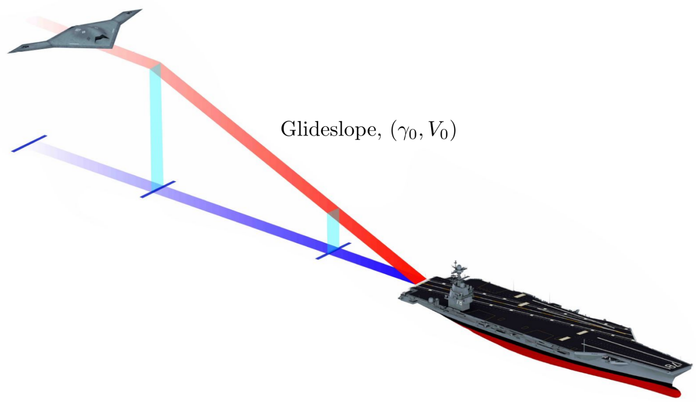

Fig. 1 Schematic representing a standard carrier landing approach profile. This includes the glideslope trajectory, defined by a flight path angle γ_0 and nominal velocity V_0, which is used to guide the UAV into the final landing maneuver.

angle is zero when the vector is parallel to the horizontal, such that $\theta_0 = \alpha_0 + \gamma_0$.

Figure 3 shows the relationship between the relative frame $\mathcal{R}$ and the body-fixed frame $\mathcal{B}$. The coordinates δp_x, δp_z, and $\delta\theta$ are with respect to the relative frame $\mathcal{R}$. The dynamics of the UAV, described in Section III, will be written with respect to the relative frame.

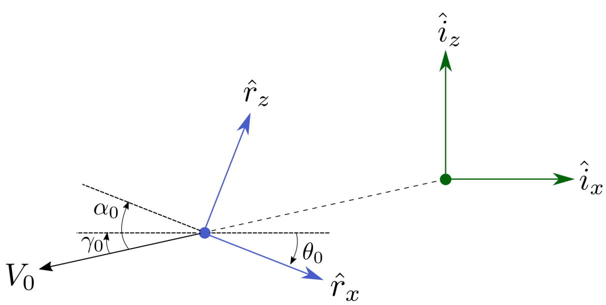

Fig. 2 Relationship between the earth-fixed frame $\mathcal{I}$ and the (inertial) relative frame $\mathcal{R}$.

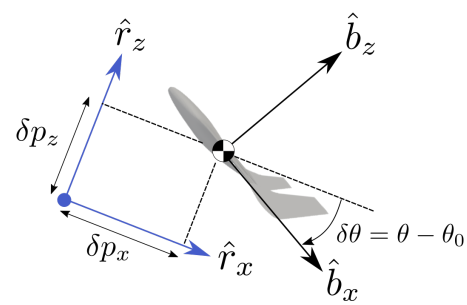

Fig. 3 Relationship between the (inertial) relative frame $\mathcal{R}$ and the body-fixed frame $\mathcal{B}$.

III. UAV Dynamics Model

Now that the relevant reference frames have been defined, we can discuss the dynamics model for the UAV system. While classical approaches to modeling aircraft dynamics typically require aerodynamic coefficients regressed from data, we use a principled CFD model of the aerodynamics that is directly coupled with the rigid-body motion. This model is then exploited in the construction of the control scheme in Section IV.

A. Aerodynamics

In this work we assume inviscid, compressible flow, neglect atmospheric changes in altitude, and write the fluid dynamics using the Arbitrary Lagrangian Eulerian (ALE) framework for mesh motion, following the approach discussed in [21]. The compressible Euler equations are therefore written in a semi-discretized form as

$$\frac{\partial}{\partial t}\left(\mathbf{A}(\delta\xi)w\right) + \mathbf{F}(w, \delta\xi, \delta\dot{\xi}) = 0,$$

where $w \in \mathbb{R}^{n_{\text{CFD}}}$ is the discretized fluid state vector, $\delta\xi \coloneqq [\delta p_x, \delta p_z, \delta\theta]^T \in \mathbb{R}^3$ is the rigid-body state vector written with respect to the relative frame, $\mathbf{A} \in \mathbb{R}^{n_{\text{CFD}} \times n_{\text{CFD}}}$ is a diagonal matrix of cell volumes, and $\mathbf{F} \in \mathbb{R}^{n_{\text{CFD}}}$ is the flux function. Additionally, the first term can be expanded to yield

$$\mathbf{A}(\delta\xi)\dot{w} + \mathbf{E}(w)\delta\dot{\xi} + \mathbf{F}(w, \delta\xi, \delta\dot{\xi}) = 0. \quad (1)$$

B. Longitudinal Rigid-Body Dynamics

The force and moment vectors acting at the center of mass of the UAV, written in relative frame coordinates, are given by

$$F = \big(-T_c\cos(\delta\theta) + mg\sin(\theta_0) + f^{\text{aero}}_{\hat{r}_x}(w)\big)\hat{r}_x + \big(T_c\sin(\delta\theta) - mg\cos(\theta_0) + f^{\text{aero}}_{\hat{r}_z}\big)\hat{r}_z, \quad M = \big(M_c + T_c\Delta z_{T_c} + M^{\text{aero}}\big)\hat{r}_y,$$

where T_c is the thrust control input, m is the UAV mass, g is acceleration due to gravity, $f^{\text{aero}} \in \mathbb{R}^2$ represents the aerodynamic force vector in relative frame coordinates, M_c is the moment control input, Δz_{T_c} is the perpendicular offset of the thrust vector with respect to the center of mass, and M^{aero} represents the aerodynamic moments in the relative frame. The resulting rigid-body dynamics are therefore given by

$$\begin{aligned} m\delta\ddot{p}_x &= -T_c\cos(\delta\theta) + mg\sin(\theta_0) + f^{\text{aero}}_{\hat{r}_x} + d_x, \\ m\delta\ddot{p}_z &= T_c\sin(\delta\theta) - mg\cos(\theta_0) + f^{\text{aero}}_{\hat{r}_z} + d_z, \\ J_y\delta\ddot{\theta} &= M_c + T_c\Delta z_{T_c} + M^{\text{aero}} + d_\theta, \end{aligned} \tag{2}$$

where J_y is the moment of inertia about the $\hat{r}_y$ axis and $d_{(\cdot)}$ is an exogenous disturbance.

C. Glideslope Linearization

Given the desired flight path angle γ_0 and desired velocity V_0, the constant motion of the relative frame with respect to the earth-fixed frame is defined. The angular offset θ_0 is then chosen as the equilibrium pitch angle for the UAV corresponding to that glideslope. Therefore with respect to the relative frame, the desired equilibrium requires $\delta\ddot{\xi}_0 = \delta\dot{\xi}_0 = \delta\xi = 0$ and the remaining equilibrium quantities are given by $T_{c,0}$, $M_{c,0}$, and w_0 for the thrust input, moment input, and fluid state respectively.

Linearizing the fluid dynamics equations (1) about this glideslope equilibrium results in

$$\mathbf{A}_0\delta\dot{w} + \mathbf{H}_0\delta w + \mathbf{C}_0\delta\dot{\xi} + \mathbf{G}_0\delta\xi = 0, \tag{3}$$

where $\mathbf{A}_0 = \mathbf{A}(\delta\xi_0)$, $\mathbf{H}_0 = \frac{\partial\mathbf{F}}{\partial w}(w_0, \delta\xi_0, \delta\dot{\xi}_0)$, $\mathbf{C}_0 = \frac{\partial\mathbf{F}}{\partial\delta\dot{\xi}}(w_0, \delta\xi_0, \delta\dot{\xi}_0)$, and $\mathbf{G}_0 = \frac{\partial\mathbf{F}}{\partial\delta\xi}(w_0, \delta\xi_0, \delta\dot{\xi}_0)$.

Then, linearizing the rigid-body dynamics (2) with respect to this equilibrium gives

$$M\delta\ddot{\xi} = \mathbf{E}_0\delta\xi + \mathbf{P}_0\delta w + \mathbf{B}_0\delta\tau + \mathbf{D}_0 d, \tag{4}$$

where $\delta\tau := [\delta T_c, \delta M_c]^T$ with $\delta T_c = T_c - T_{c,0}$ and $\delta M_c = M_c - M_{c,0}$ denotes the deviation in control from the equilibrium values, $\delta w = w - w_0$ is the fluid state perturbation, $d := [d_x, d_z, d_\theta]^T$ is the disturbance vector and

$$M = \begin{bmatrix} m & 0 & 0 \\ 0 & m & 0 \\ 0 & 0 & J_y \end{bmatrix}, \quad \mathbf{E}_0 = \begin{bmatrix} 0 & 0 & 0 \\ 0 & 0 & T_{c,0} \\ 0 & 0 & 0 \end{bmatrix} + \begin{bmatrix} \frac{\partial f^{\text{aero}}_{\hat{r}_x}}{\partial\delta\xi}\big|_0 \\ \frac{\partial f^{\text{aero}}_{\hat{r}_z}}{\partial\delta\xi}\big|_0 \\ \frac{\partial M^{\text{aero}}}{\partial\delta\xi}\big|_0 \end{bmatrix}, \quad \mathbf{P}_0 = \begin{bmatrix} \frac{\partial f^{\text{aero}}_{\hat{r}_x}}{\partial w}\big|_0 \\ \frac{\partial f^{\text{aero}}_{\hat{r}_z}}{\partial w}\big|_0 \\ \frac{\partial M^{\text{aero}}}{\partial w}\big|_0 \end{bmatrix}, \quad \mathbf{B}_0 = \begin{bmatrix} -1 & 0 \\ 0 & 0 \\ \Delta z_{T_c} & 1 \end{bmatrix}, \quad \mathbf{D}_0 = I$$

where $(\cdot)|_0$ denotes a quantity evaluated at the equilibrium state.

D. Full Order Model

The linear, full order model (FOM) of the UAV system can now be defined using the coupled equations (3) and (4). Defining the state vector $x^f := [\delta\xi, \delta\dot{\xi}, \delta w]^T \in \mathbb{R}^{n^f}$ where $n^f = 6 + n_{\text{CFD}}$, and the control vector $u := \delta\tau \in \mathbb{R}^m$ where $m = 2$, the dynamics for the UAV are given by

$$\dot{x}^f = A^f x^f + B^f u + B^f_d d, \quad A^f = \begin{bmatrix} 0 & I & 0 \\ M^{-1}\mathbf{E}_0 & 0 & M^{-1}\mathbf{P}_0 \\ -\mathbf{A}_0^{-1}\mathbf{G}_0 & -\mathbf{A}_0^{-1}\mathbf{C}_0 & -\mathbf{A}_0^{-1}\mathbf{H}_0 \end{bmatrix}, \quad B^f = \begin{bmatrix} 0 \\ M^{-1}\mathbf{B}_0 \\ 0 \end{bmatrix}, \quad B^f_d = \begin{bmatrix} 0 \\ M^{-1}\mathbf{D}_0 \\ 0 \end{bmatrix} \tag{5}$$

where I is the appropriately sized identity matrix. Additionally, it is assumed that measurements of the rigid-body state $(\delta\xi, \delta\dot{\xi})$ are available and therefore a measurement model is given by

$$y^f = C^f x^f + v, \quad C^f = \begin{bmatrix} I & 0 \end{bmatrix}, \tag{6}$$

where $y^f \in \mathbb{R}^p$ with $p = 6$ is the measurement vector and $v \in \mathbb{R}^p$ represents the measurement noise.

E. Reduced Order Model

High-fidelity CFD models require fine spatial discretizations, which result in very high-dimensional fluid state vectors δw and coupled dynamics models defined by (5). This poses a significant challenge to controller design, which we show can be overcome by designing the controller based on a reduced order model.

Using a projection-based model order reduction method (i.e. balanced truncation or POD), the Petrov-Galerkin projection matrices $V \in \mathbb{R}^{n^f \times n}$ and $W \in \mathbb{R}^{n^f \times n}$ can be defined where $n \ll n^f$. The projection matrix $P = V(W^T V)^{-1} W^T$ can then be used to project a vector in $\mathbb{R}^{n^f}$ onto the subspace spanned by the columns of V, and the low-dimensional approximation of x^f is given by $x \in \mathbb{R}^n$ where $x^f \approx Vx$. Substituting $x^f = Vx$ in the full order model (5) and left multiplying by the matrix $(W^T V)^{-1} W^T$ then gives

$$\dot{x} = A^r x + B^r u, \quad A^r = (W^T V)^{-1} W^T A^f V, \quad B^r = (W^T V)^{-1} W^T B^f, \tag{7}$$

which is referred to as the reduced order model and the state vector x is referred to as the reduced order state. Note that we have omitted the disturbance term as they are unknown and since we will only use this reduced order model for *nominal* trajectory planning. A reduced order measurement model can also be defined, and is given by

$$y = C^r x + v, \quad C^r = C^f V, \tag{8}$$

where $y \in \mathbb{R}^6$ is an approximation of the true measurement vector y^f.

IV. CFD-Based Model Predictive Control

A. Control Problem Definition

As mentioned in Section II, the overall objective is to design a controller that enables the UAV to track the desired glideslope while obeying constraints that are imposed on the UAV's rigid-body state and control inputs. These constraints are assumed to be expressed as

$$z^f \in \mathcal{Z}, \quad u \in \mathcal{U}, \tag{9}$$

where $z^f = H^f x^f$ will be referred to as performance variables and $\mathcal{Z} := \{z^f \mid H_z z^f \leq b_z\}$ and $\mathcal{U} := \{u \mid H_u u \leq b_u\}$ are compact, convex polytopes that contain the origin. Additionally, we choose $H^f = C^f$ such that the performance variables correspond to the rigid-body states (i.e. position, velocity, pitch angle, and pitch rate). We also make the assumption that the disturbances that act on the UAV satisfy

$$d \in \mathcal{D}, \quad v \in \mathcal{V}, \tag{10}$$

where $\mathcal{D} := \{d \mid H_d d \leq b_d\}$ and $\mathcal{V} := \{v \mid H_v v \leq b_v\}$ are compact, convex polytopes that contain the origin.

As the system dynamics have been expressed with respect to the relative frame (which moves along the glideslope at the desired velocity), glideslope trajectory tracking is accomplished by driving the coupled system (5) to its origin. The cost of a given trajectory that the system takes is then evaluated by the tunable cost function

$$J = \int_0^\infty (x^f)^T Q^f x^f + u^T R^f u \, dt, \tag{11}$$

where Q^f and R^f are positive definite weighting matrices, and ideally the controller should be designed to minimize J.

As discussed previously, model predictive control is a powerful framework for approaching constrained optimal control problems such as this. In this work we use an implicit MPC framework, which requires the online solution of optimization problems typically formulated as quadratic programs (QPs). Standard off-the-shelf interior-point methods for solving these QPs generally require $O\big((n_x + n_u)^3\big)$ operations per step with respect to the state and control dimensions n_x and n_u [22], which for moderately sized problems is computationally tractable. However, designing an MPC scheme based on the FOM (5) would be intractable for real-time control since $n^f \gg 1$.

Therefore, we propose to use the reduced order model (7) to design a computationally efficient MPC scheme that still exploits the fidelity of the full order CFD model. Our proposed MPC scheme consists of three main components: (a) a constrained optimal control problem using the reduced order model that defines a nominal open-loop trajectory, (b) a state estimator that computes an estimate of the reduced order state from the available measurements, and (c) an ancillary linear feedback control term that uses the reduced order state estimate to close the loop and drive the UAV to track the nominal trajectory. The reduced order MPC (ROMPC) problem that produces the nominal trajectory is defined in Section IV.B, followed by definition of the state estimator in Section IV.C, and finally the UAV control law is defined in Section IV.D.

B. Reduced Order Model Predictive Controller

The ROMPC problem produces a trajectory for a simulated nominal ROM system

$$\dot{\bar{x}} = A^r \bar{x} + B^r \bar{u}, \quad \bar{y} = C^r \bar{x}, \quad \bar{z} = H^r \bar{x}, \tag{12}$$

where $\bar{z}_k$ are the reduced order performance variables and $H^r = H^f V = C^r$. Note that the input $\bar{u}$ to this simulated system is not the same as the input u to the UAV, but their relationship is given by the control law in Section IV.D. To design the ROMPC problem, a discrete-time version of (12) is given by

$$\bar{x}_{k+1} = A\bar{x}_k + B\bar{u}_k, \quad \bar{y}_k = C\bar{x}_k, \quad \bar{z}_k = H\bar{x}_k, \tag{13}$$

where $A = e^{\Delta t A^r}$, $B = \big(\int_0^{\Delta t} e^{\tau A^r} d\tau\big)B^r$, $C = C^r$, and $H = H^r$ are the discrete equivalents assuming a zero-order hold input, k is the discrete time index, and Δt is the discretization time step.

The ROMPC problem is then defined using a standard MPC formulation to compute the control inputs $\bar{u}_k$ for the discrete-time ROM (13). Specifically the ROMPC problem computes at each time step $k \in \mathbb{Z}_{\geq 0}$ a trajectory over a finite horizon $N \in \mathbb{Z}_{>0}$, given by the state and control sequences $\bar{\mathbf{x}}^*_{\mathbf{k}} := [\bar{x}^*_{k|k}, \dots, \bar{x}^*_{k+N|k}]$ and $\bar{\mathbf{u}}^*_{\mathbf{k}} := [\bar{u}^*_{k|k}, \dots, \bar{u}^*_{k+N-1|k}]$. The notation $(\cdot)_{i|k}$ denotes the trajectory quantity associated with time $i \in [k, \dots, k+N]$ computed at time k, and the notation $(\cdot)^*$ denotes optimality with respect to the defined cost function and associated constraints. At each time step the control $\bar{u}_k$ is then given by $\bar{u}_k = \bar{u}^*_{k|k}$ and the input $\bar{u}$ to the continuous time ROM (12) is the zero-order hold of $\bar{u}^*_{k|k}$ over the discretization time step. The ROMPC optimization problem computed at time k is defined as

$$\begin{aligned}
(\bar{\mathbf{x}}^*_{\mathbf{k}}, \bar{\mathbf{u}}^*_{\mathbf{k}}) := \underset{\bar{\mathbf{x}}_{\mathbf{k}}, \bar{\mathbf{u}}_{\mathbf{k}}}{\arg\min.} \;\; & ||\bar{x}_{k+N|k}||^2_P + \sum_{j=k}^{k+N-1} ||\bar{x}_{j|k}||^2_Q + ||\bar{u}_{j|k}||^2_R, \\
\text{subject to} \;\; & \bar{x}_{i+1|k} = A\bar{x}_{i|k} + B\bar{u}_{i|k}, \\
& \bar{z}_{i|k} = H\bar{x}_{i|k} \\
& \bar{z}_{i|k} \in \bar{\mathcal{Z}}, \;\; \bar{u}_{i|k} \in \bar{\mathcal{U}}, \\
& \bar{x}_{k+N|k} \in \bar{\mathcal{X}}_f, \;\; \bar{x}_{k|k} = \bar{x}_k,
\end{aligned} \tag{14}$$

where $i = k, \dots, k+N-1$ and the decision variables are the nominal trajectory quantities $(\bar{\mathbf{x}}_{\mathbf{k}}, \bar{\mathbf{u}}_{\mathbf{k}})$. It is important to note that the initial condition constraint uses $\bar{x}_k$, which is the current state of the discrete ROM (13) that is initialized as $\bar{x}_0 = \bar{x}(0)$. The cost function is quadratic and is defined by the positive definite penalty weighting matrices P, Q, and R where we choose $Q = V^T Q^f V$ and $R = R^f$ to attempt to minimize the true cost function (11). The terminal cost weighting matrix P, along with the convex polytopic terminal set $\bar{\mathcal{X}}_f$, are designed using the techniques presented in [10] in order to guarantee recursive feasibility and exponential stability of the controlled discrete-time ROM (i.e. convergence of (13) to the origin under the control $\bar{u}_k = \bar{u}^*_{k|k}$). Finally, the constraint sets $\bar{\mathcal{Z}}$ and $\bar{\mathcal{U}}$ are *tightened* versions of the constraints sets $\mathcal{Z}$ and $\mathcal{U}$ from (9). Constraint tightening is a common technique in classical tube-based robust MPC to account for unpredictable disturbances that might make the controlled system deviate from the nominal trajectory planned by the MPC scheme. In our case the tightening also takes into account the model reduction error induced by using the ROM in the MPC scheme. A more thorough discussion on the computation of $\bar{\mathcal{Z}}$ and $\bar{\mathcal{U}}$ is given in Section IV.E.

C. Reduced Order State Estimator

Now that the ROMPC problem (14) is defined the reduced order state estimator is introduced. This estimator, which is also based on the ROM (13) for computational efficiency, is defined by

$$\dot{\hat{x}} = A^r \hat{x} + B^r u + L(y^f - C^r \hat{x}), \tag{15}$$

where $\hat{x}$ is the reduced order state estimate, y^f is the measurement of the UAV rigid-body state given by (6), u is the control applied to the UAV, and L is the estimator gain matrix.

D. Reduced Order Controller

The control law that is applied to the UAV system is then defined for $t \in [k\Delta t,\ (k+1)\Delta t]$ as

$$u = \bar{u}^*_{k|k} + K(\hat{x} - \bar{x}), \tag{16}$$

where $\bar{u}^*_{k|k}$ is the zero-order hold input to the continuous time ROM computed by the ROMPC problem (14) at time k, $\bar{x}$ is the state of the continuous time ROM under the zero-order hold input $\bar{u} = \bar{u}^*_{k|k}$, and K is the controller gain matrix.

E. Robustness and Stability Guarantees

We now address in more detail the performance of the control scheme, focusing on guarantees of constraint satisfaction and stability of the real UAV system while accounting for the error induced by the use of the reduced order model, disturbances acting on the system, and state estimation error. To guarantee robust constraint satisfaction we use the method proposed by [20] where we consider the approximation error $e = x^f - V\bar{x}$ and the control error $d = \hat{x} - \bar{x}$ whose joint dynamics are given by

$$\dot{\epsilon} = A_\epsilon \epsilon + B_\epsilon r + G_\epsilon \omega, \quad A_\epsilon = \begin{bmatrix} A^f & B^f K \\ LC^f & A^r + B^r K - LC^r \end{bmatrix}, \quad B_\epsilon = \begin{bmatrix} P_\perp A^f V & P_\perp B^f \\ 0 & 0 \end{bmatrix}, \quad G_\epsilon = \begin{bmatrix} B^f_d & 0 \\ 0 & L \end{bmatrix}, \tag{17}$$

where $P_\perp = I - V(W^T V)^{-1} W^T$, $r = [\bar{x}^T,\ \bar{u}^T]^T$, and $\omega = [d^T,\ v^T]^T$. Note that in these continuous time dynamics the term $\bar{x}$ represents the continuous time trajectory of the nominal ROM (7) and where the control $\bar{u}$ is the zero-order hold of the control computed by the ROMPC problem in Section IV.B.

We now make the assumption that over the time interval $[k\Delta t,\ (k+1)\Delta t]$ the quantities $\bar{x}$, d, and v are constant and compute the discrete equivalent of the error dynamics assuming a zero-order hold. With this discrete equivalent the method described in [20] can be used to compute the tightened constraint sets $\bar{\mathcal{Z}}$ and $\bar{\mathcal{U}}$ that are used in the ROMPC problem. In particular, these tightened sets are computed by finding bounds on how much the constraints might be violated due to disturbances, state estimation error, and model reduction error.

This method also requires some additional assumptions, including that A_ϵ is a stable matrix, that the initial error $\epsilon(0)$ is bounded, and that the nominal ROM system satisfies the constraints $\bar{z} \in \mathcal{Z}$, $\bar{u} \in \mathcal{U}$ for a predefined "burn in" period before the constraint satisfaction guarantees are valid. The first assumption can be satisfied by appropriately choosing the gain matrices K and L, and the others can be satisfied in practice by initializing the simulated continuous time ROM (12) and state estimator (15) before the glideslope sequence begins to give them time to converge.

For an analysis of stability and convergence of the closed loop system we use the results from [20]. Specifically we note that since the gain matrices K and L are designed such that A_ϵ is a stable matrix and since the ROMPC controller is designed such that the nominal ROM exponentially converges to the origin, then in the disturbance free scenario the error $\epsilon \to 0$ which in turn implies that $x^f \to 0$ and $\hat{x} \to 0$.

V. UAV Glideslope Tracking

We now present simulation results that demonstrate the capabilities of our proposed CFD-based MPC scheme. For this problem we utilize a model of the mAEWing2 [23] shown in Figure 4, for which the methods presented in Section III.A were used to build a CFD model with 2,082 nodes and a fluid state vector with $n_{\text{CFD}} = 10{,}410$. The glideslope to be tracked is defined by a flight path angle $\gamma_0 = -3.5°$ and a nominal velocity of $V_0 = 30.48$ m/s. The dynamic equilibrium of the UAV corresponding to this glideslope is defined by an equilibrium pitch angle of $\theta_0 \approx -2.9°$, an equilibrium thrust of $T_0 \approx 147$ N, and an equilibrium pitch moment of $M_0 \approx 14$ Nm. Both the fluid and rigid-body dynamics are linearized using these equilibrium conditions to give a linear FOM for the coupled rigid-body/fluid system given by (5) where $n^f = 10{,}416$. A visualization of the pressure distribution generated by the fluid across the surface of the UAV at this equilibrium condition is given in Figure 10. It is interesting to note that for this UAV the coupled rigid-body/fluid dynamics are *unstable*.

The constraints imposed on the rigid-body state and control include

$$\begin{aligned} &|\delta p_x| \le 50 \text{ m}, \quad |\delta p_z| \le 10 \text{ m}, \quad |\delta\theta| \le 10°, \\ &|\delta \dot{p}_x| \le 20 \text{ m/s}, \quad |\delta \dot{p}_z| \le 5 \text{ m/s}, \quad |\delta\dot{\theta}| \le 10°/\text{s}, \\ &|\delta T_c| \le 100 \text{ N}, \quad |\delta M_c| \le 50 \text{ Nm}, \end{aligned}$$

which define the polytopes $\mathcal{Z}$ and $\mathcal{U}$. The assumed bounds on the disturbances are given by

$$|d_x| \le 1 \text{ N}, \quad |d_z| \le 10 \text{ N}, \quad |d_\theta| \le 0.1 \text{ Nm},$$

to account for wind gusts or other disturbances that effect the rigid-body dynamics and

$$|v_{\delta p_x}| \leq 0.1 \text{ m}, \quad |v_{\delta p_z}| \leq 0.1 \text{ m}, \quad |v_{\delta\theta}| \leq 0.5^\circ,$$
$$|v_{\delta \dot{p}_x}| \leq 0.1 \text{ m/s}, \quad |v_{\delta \dot{p}_z}| \leq 0.1 \text{ m/s}, \quad |v_{\delta\dot{\theta}}| \leq 1^\circ\text{/s},$$

where $v_{(\cdot)}$ denotes the noise associated with the measurement of the rigid-body state $(\cdot)$. For simplicity the cost function (11) is defined with Q^f and R^f both being diagonal and where the first six elements of Q^f (associated with the rigid-body state perturbations) are chosen to be [10, 10, 1000, 100, 100, 100] and the remaining diagonal terms set to 0.001. The control penalty R^f is simply chosen to be $R^f = I$. No cost function tuning was performed for this problem.

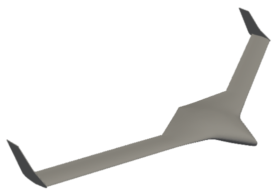

Fig. 4 The mAEWing2 model used to develop the CFD aerodynamics model for the results presented in Section V.

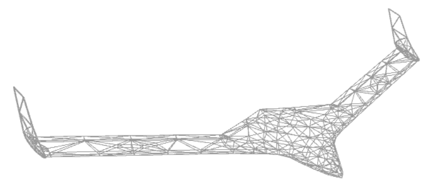

Fig. 5 The surface mesh of the mAEWing2 CFD model, which in total contained 2,082 nodes.

A. Model Reduction

The CFD model given by (3) is reduced using balanced truncation where the terms including the rigid-body states are considered inputs and the effect of the fluid on the rigid-body states (i.e. the $\mathbf{P}_0\delta w$ term from (4)) are considered the system output. Balanced truncation [16] is used as it is a principled technique applicable to stable systems that intuitively seeks to capture the most controllable and observable modes of the system, and has the nice theoretical property that the $\mathcal{H}_\infty$-norm of the error system can be bounded by the sum of the neglected Hankel singular values (which can be used as a metric for the quality of the model reduction). For the CFD model of the mAEWing2 UAV we choose $n_{\text{ROM}} = 20$, such that the sum of the neglected Hankel singular values is approximately 0.1% of the total sum, and we denote the model reduction matrices V_{CFD} and W_{CFD}.

Once the CFD model is reduced it is coupled with the rigid-body dynamics to yield a ROM with dimension $n = 26$. Note that this coupled system can also be defined as the model reduction of the FOM (5) where the model reduction matrices are

$$V = \begin{bmatrix} I & 0 \\ 0 & V_{\text{CFD}} \end{bmatrix}, \quad W = \begin{bmatrix} I & 0 \\ 0 & W_{\text{CFD}} \end{bmatrix}.$$

As we mentioned previously the coupled FOM is unstable (even though the fluid sub-system is stable), and therefore it is not surprising that the coupled ROM is also unstable.

Note that in this particular case balanced truncation is a computationally viable option since the FOM only has around 10,000 degrees of freedom. However for increased resolution or more complex fluid problems (e.g. including viscosity effects), the resulting CFD models may have millions of degrees of freedom. Reducing these models with balanced truncation is not computationally tractable and therefore in the future we would like to also consider models generated using data-driven techniques such as POD [24].

B. Controller Design

Once the ROM is defined, the controller and estimator gains K and L are chosen such that A_ϵ is a stable matrix. This is accomplished by defining the cost matrices $Q = V^T Q^f V$ and $R = R^f$ and choosing K and L as the infinite horizon linear quadratic regulator gains based on the ROM dynamics. This method for defining K and L is chosen because in the case that $A^r = A^f$, $B^r = B^f$ and $C^r = C^f$ the separation principle can be used to make the A_ϵ block triangular with diagonal blocks $A^f + B^f K$ and $A^f - LC^f$. Therefore our choice of K and L is guaranteed to make A_ϵ stable. While no guarantees can be made that this procedure will make A_ϵ stable when using the actual ROM dynamics, the approach seems to work well in practice and can be validated by simply computing the eigenvalues of A_ϵ.

Next we compute the tightened constraint sets $\bar{\mathcal{Z}}$ and $\bar{\mathcal{U}}$ for the ROMPC problem as discussed in Section IV.E. Specifically, using the method from [20] we choose $\tau = 1000$, compute M and γ by eigenvalue decomposition, G is computed using the geometric programming approach (solved with batch coordinate descent), and C_r and C_w are computed using vertex enumeration. Since this method requires the assumption that the ROM satisfies the constraints $\mathcal{Z}$ and $\mathcal{U}$ for a predefined burn-in period we also increase the constraints on $|\delta p_x|$ and $|\delta p_z|$ (for error computation only) to be less than 500 since they are integrator modes and therefore may not stay within a small region before the control scheme is activated. However these bounds will still be valid to tighten the actual constraint sets $\mathcal{Z}$ and $\mathcal{U}$.

Additionally, the time discretization of the error system as discussed in Section IV.E is performed using $\Delta t = 0.05$ s, which is also the time step used to discretize the ROM for the ROMPC problem. Finally, as mentioned in Section IV.B the terminal cost and terminal set P and $\bar{\mathcal{X}}_f$ are computed using standard techniques from [10], the cost matrices Q and R are the same used to compute K and L, and the time horizon is chosen to be $N = 20$ (corresponding to 1 second).

The tightened constraints in the ROMPC problem, computed using the method from [20], are given in Table 1. In particular, the first row shows the original constraints which define $\mathcal{Z}$ and $\mathcal{U}$, the second row shows the tightened constraints that define $\bar{\mathcal{Z}}$ and $\bar{\mathcal{U}}$ used in the ROMPC scheme, the third row shows the bounds on the constraint violations computed by the method from [20] that are used to tighten the constraints, and the fourth row shows the percent of those bounds that are a result of the exogenous disturbances d and v that act on the system. It is interesting to see that in the $\hat{r}_x$

	$\lvert\delta p_x\rvert$	$\lvert\delta p_z\rvert$	$\lvert\delta\theta\rvert$	$\lvert\delta\dot{p}_x\rvert$	$\lvert\delta\dot{p}_z\rvert$	$\lvert\delta\dot{\theta}\rvert$	$\lvert\delta T_c\rvert$	$\lvert\delta M_c\rvert$
Original Constraint	50 m	10 m	10°	20 m/s	5 m/s	10°/s	100 N	50 Nm
Tightened Constraint	28.9 m	8.0 m	8.0°	13.2 m/s	4.0 m/s	3.3°/s	32.8 N	41.4 Nm
Difference (Error Bounds)	21.1 m	2.0 m	2.0°	6.8 m/s	1.0 m/s	6.7°/s	67.2 N	8.6 Nm
% From Disturbances	4%	55%	51%	4%	57%	64%	5%	43%

Table 1 Comparison between original and tightened constraints.

direction (specifically δp_x, $\delta\dot{p}_x$, and δT_c) the amount of constraint tightening due to errors from model reduction and state estimation are much higher (around 95% of the total) while for the other constraints the tightening due to errors from model reduction and state estimation are approximately equal to the errors from the exogenous disturbances. This could be a result of model reduction error, but it is likely also an effect of the chosen gain matrix K.

C. Simulation

Using the control scheme discussed in Section V.B the *full order* linearized coupled rigid-body/fluid model (5) can be simulated with the controller in the loop. This simulation is performed by integrating the continuous time FOM using an implicit backwards-Euler scheme with a time step of 0.01 seconds. The control input (16) is also computed every 0.01 seconds by also updating the nominal ROM state $\bar{x}$ and state estimate $\hat{x}$ at the same rate. As mentioned before the discrete time ROM was designed assuming a zero-order hold over $\Delta t = 0.05$ s and therefore the ROMPC problem is only solved once every 5 steps in the simulation.

1. Scenario A

To demonstrate the performance of the controller, the system is first initialized at an equilibrium condition with $\delta p_x = 10$ m and $\delta p_z = -5$ m, and the controller's simulated ROM and state estimator are also initialized at their corresponding equilibrium conditions with the same positions δp_x and δp_z. This initial condition corresponds to the UAV following a glideslope with the same desired speed V_0 and flight path angle γ_0, but shifted with respect to the Earth-fixed inertial frame $\mathcal{I}$. Figure 6 shows results from a simulation with no external disturbances and where the nominal ROM trajectory computed by the ROMPC problem is also shown, and Figure 7 shows the case where the UAV is also subject to external disturbances described earlier in this section, where at each time step the disturbance vectors are drawn randomly from a uniform distribution. In these simulations the average time to solve the ROMPC QP using CPLEX was approximately 0.04 seconds on a machine with a 2.5 GHz Intel Core i5 processor and 8GB of memory.

As can be seen in Figure 6 the system converges to the origin as desired and satisfies the constraints. Note that in this particular case the tightened constraint $|\delta\dot{\theta}| \leq 3.3°$/s is active in the ROMPC problem at the beginning of the simulation. We can also see that the UAV tracks the trajectory defined by the ROMPC problem very well, except for δp_x and $\delta\dot{p}_x$ which has some error. This aligns with our observations from the error bound results in Table 1 where we saw that the error bounds for these variables were significantly larger than than the others. We hypothesize that this is more

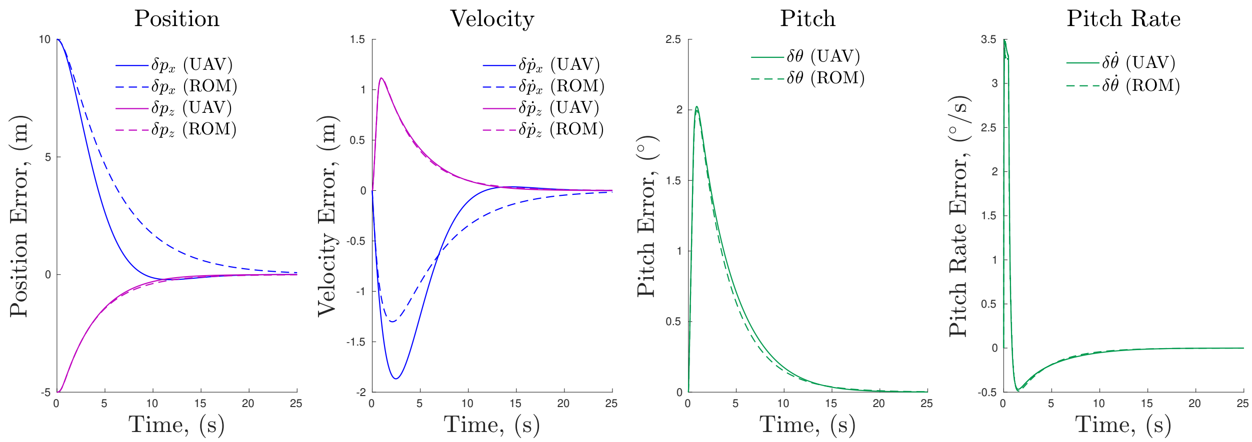

Fig. 6 Results from the Section V.C.1 simulation of the linear CFD-based full order model for the mAEWing2 UAV without disturbances.

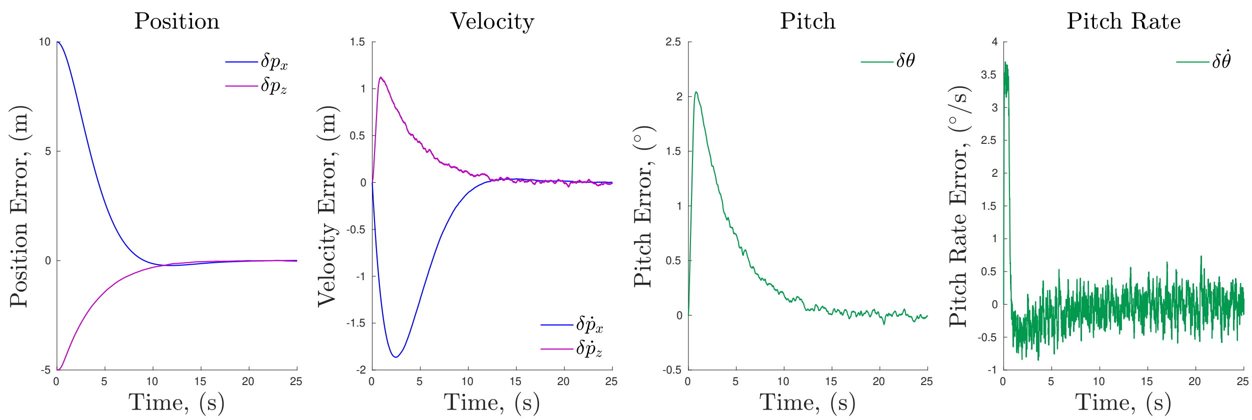

Fig. 7 Results from the Section V.C.1 simulation of the linear CFD-based full order model for the mAEWing2 UAV with sensor noise and external disturbances.

of a result of the choice of the controller gains K than it is due to model reduction error, and exploring this observation further as well as more robust options for choosing K and L is planned future work. In Figure 7 we see the effect of the disturbances and sensor noise on the UAV. Since the assumed bounds on the disturbances d presented at the beginning of this section are much larger for d_z we would expect to see the larger deviations in $\delta \dot{p}_z$ than in $\delta \dot{p}_x$, and we can also see the effect of the moment disturbances d_θ quite clearly in the pitch and pitch rate trajectories.

2. Scenario B

To consider another realistic scenario we also simulate the case where the UAV has intercepted the desired glideslope trajectory defined by (V_0, γ_0), but is currently flying at an equilibrium condition corresponding to a glideslope trajectory given by (V, γ) where $V = 35$ m/s and $\gamma = -2°$. In other words the UAV is approaching with too shallow of a trajectory and is 5 m/s too fast. We also initialize the state estimator and the nominal ROM in a more general way. Specifically we start the simulation 50 seconds before the glideslope is intercepted and the CFD-based control scheme is applied, and initialize $\bar{x} = \hat{x}$ where the rigid-body states in $\hat{x}$ are set using the current UAV rigid-body state measurement y^f and the reduced order fluid states are initialized to be zero. Note that during this period the control for the ROM system is defined as $\bar{u} = u - K(\hat{x} - \bar{x})$ where u is the control being applied to the UAV. Once again we run a simulation with and without the disturbances acting on the system, which are shown in Figures 8 and 9, respectively. Once again, in these simulations the average time to solve the ROMPC problem was approximately 0.04 seconds.

First, to evaluate the effect of initializing the state estimator and ROM as described we consider their initial conditions

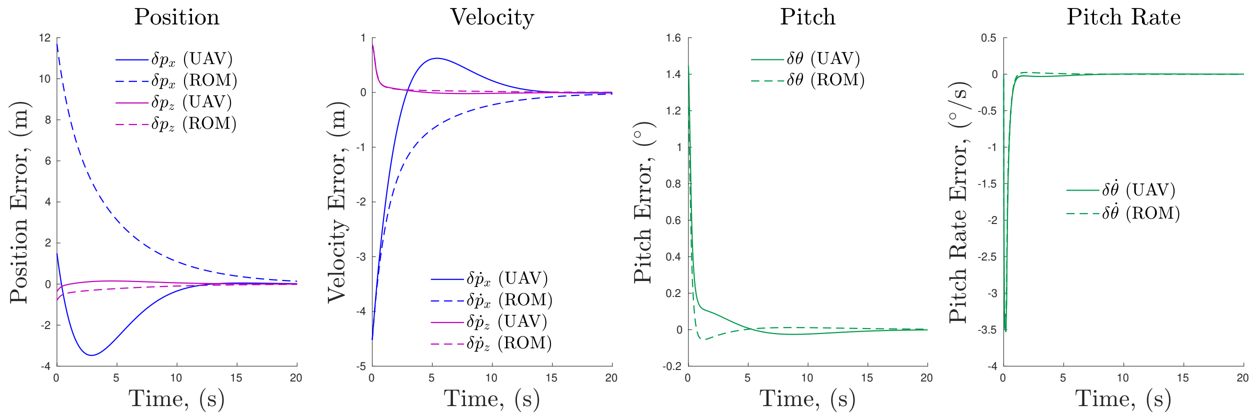

Fig. 8 UAV simulation results for the scenario discussed in Section V.C.2, without disturbances.

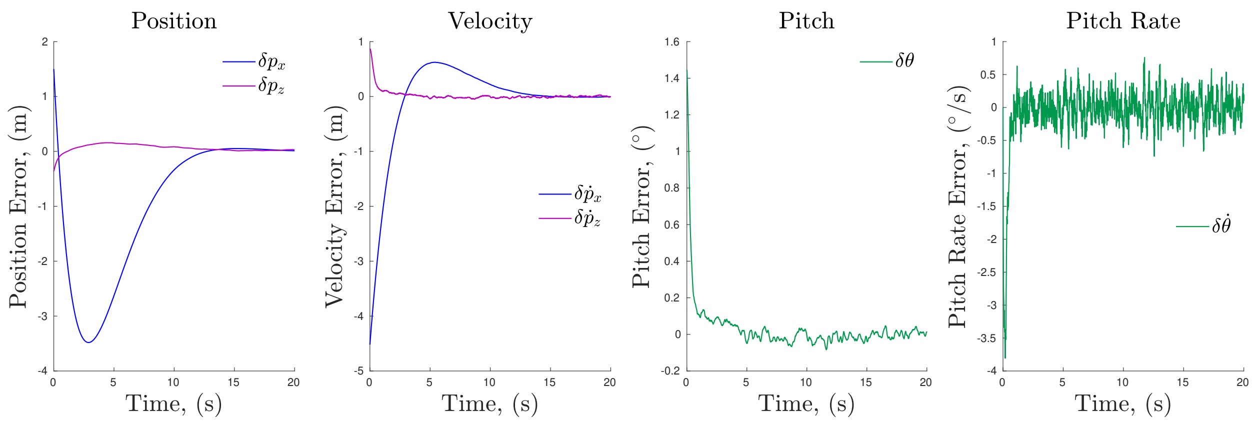

Fig. 9 UAV simulation results for the scenario discussed in Section V.C.2, with sensor noise and external disturbances.

when the proposed control scheme takes over the track the desired glideslope, which occur at $t = 0$ in Figures 8 and 9. We can see that at $t = 0$ the ROM's rigid-body states closely match the UAV's rigid-body states except for δp_x (however as expected the error is still smaller than the 21.1 m bound presented in Table 1), which seems to follow a similar trend as seen in Section V.C.1 that we hypothesize is caused by the choice of K. However, even in the presence of the initial condition error we can see that the UAV converges to the origin and tracks the ROMPC trajectory quite well, and certainly satisfies the bounds presented in Table 1. Once again we also provide results when disturbances are included, presented in Figure 9, where we see that the UAV noisily converges to the origin.

VI. Conclusion

This work presents a CFD-based MPC scheme for controlling a UAV during autonomous aircraft carrier landing maneuvers, namely for the glideslope tracking problem. While classical MPC schemes are computationally constrained to using low-fidelity models of the UAV aerodynamics, we have shown that high-fidelity CFD models can be incorporated through the use of projection-based reduced order modeling. Specifically, a CFD-based model predictive control scheme that leverages a reduced order CFD model for the online optimization problem and the state estimator is presented and demonstrated in simulation. Through an analysis of the possible constraint violations that could arise due to the state estimation error, bounded disturbances, *and* model reduction error, the proposed control scheme is also designed such that constraint satisfaction is robustly guaranteed for the UAV.

Future Work: Additional work to improve the performance and applicability of this approach includes studying the use of different model reduction techniques as well as more rigorous methods from computing the controller gains K and L. For example, the use of proper orthogonal decomposition techniques such as in [24] should be explored so that

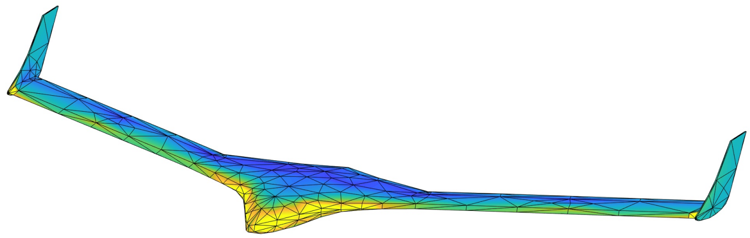

Fig. 10 Interpolated pressure distribution heat map across the UAV surface at the glideslope equilibrium state.

higher fidelity CFD models can be utilized (since balanced truncation can be computationally intensive). Regarding the controller gains, we hypothesized in the discussion on the simulation results that the choice of K and L have a significant impact on the ability of the controller to make the FOM track the nominal ROM trajectory, and therefore their design should be considered in more detail.

Acknowledgments

This work was supported by the Office of Naval Research under Grant N00014-17-1-2749, and by a research grant from the King Abdulaziz City for Science and Technology (KACST). Additionally, Joseph Lorenzetti is supported by the Department of Defense (DoD) through the National Defense Science and Engineering Fellowship (NDSEG) Program and Andrew McClellan acknowledges support from a Stanford University Graduate Fellowship.

References

[1] Dahm, W. J. A., *Technology Horizons: A Vision for Air Force Science & Technology During 2010–2030*, Air Force Research Institute, 2010.

[2] Urnes, J. M., and Hess, R. K., "Development of the F/A-18A automatic carrier landing system," *AIAA Journal of Guidance, Control, and Dynamics*, Vol. 8, No. 3, 1985, pp. 289–295.

[3] Ellis, J. D., "A Review and Analysis of Precision Approach and Landing System (PALS) Certification Procedures," Master's thesis, The Univ. of Tennessee, Knoxville, 2003.

[4] Crassidis, J., and Mook, D., "Robust control design of an automatic carrier landing system," *AIAA Astrodynamics Conference*, 1992.

[5] Niewoehner, R. J., and Kaminer, I. I., "Design of an autoland controller for an F-14 aircraft using H-infinity synthesis," *AIAA Journal of Guidance, Control, and Dynamics*, Vol. 19, No. 3, 1996, pp. 656–663.

[6] Steinberg, M. L., and Page, A. B., "A comparison of neural, fuzzy, evolutionary, and adaptive approaches for carrier landing," *AIAA Conf. on Guidance, Navigation and Control*, 2001.

[7] Denison, N. A., "Automated carrier landing of an unmanned combat aerial vehicle using dynamic inversion," Tech. rep., Air Force Institute of Technology, 2007.

[8] Ramesh, S. H., and Subbarao, K., "Autonomous Carrier Landing System for the A/V-8B Harrier like UAV," *IFAC-Papers Online*, Vol. 49, No. 1, 2016, pp. 290–295.

[9] Reed, S., and Steck, J. E., "Adaptive Control for Fault Tolerant Autonomous Carrier Recovery," *AIAA Conf. on Guidance, Navigation and Control*, 2018.

[10] Rawlings, J. B., Mayne, D. Q., and Diehl, M. M., *Model Predictive Control: Theory, Computation, and Design*, Nob Hill Publishing, 2017.

[11] Eren, U., Prach, A., Koçer, B. B., Raković, S. V., Kayacan, E., and Açikmese, B., "Model Predictive Control in Aerospace Systems: Current State and Opportunities," *AIAA Journal of Guidance, Control, and Dynamics*, Vol. 40, No. 7, 2017, pp. 1541–1566.

[12] Koo, S., Kim, S., and Suk, J., "Model Predictive Control for UAV Automatic Landing on Moving Carrier Deck with Heave Motion," *IFAC-Papers Online*, Vol. 48, No. 5, 2015, pp. 59–64.

[13] Misra, G., and Bai, X., "Stochastic Model Predictive Control for Gust Alleviation during Aircraft Carrier Landing," *American Control Conference*, 2018.

[14] Misra, G., and Bai, X., "Output-Feedback Stochastic Model Predictive Control for Glideslope Tracking During Aircraft Carrier Landing," *AIAA Journal of Guidance, Control, and Dynamics*, Vol. 42, No. 9, 2019, pp. 2098–2105.

[15] Ngo, T. D., and Sultan, C., "Model Predictive Control for Helicopter Shipboard Operations in the Ship Airwakes," *AIAA Journal of Guidance, Control, and Dynamics*, Vol. 39, No. 3, 2016, pp. 574–589.

[16] Antoulas, A., *Approximation of Large-Scale Dynamical Systems*, SIAM, 2005.

[17] Amsallem, D., Deolalikar, S., Gurrola, F., and Farhat, C., "Model Predictive Control under Coupled Fluid-Structure Constraints Using a Database of Reduced-Order Models on a Tablet," *AIAA Aviation Technology, Integration, and Operations (ATIO) Conference*, 2013.

[18] Hovland, S., Gravdahl, J. T., and Willcox, K. E., "Explicit Model Predictive Control for Large-Scale Systems via Model Reduction," *AIAA Journal of Guidance, Control, and Dynamics*, Vol. 31, No. 4, 2008, pp. 918–926.

[19] Lorenzetti, J., Landry, B., Singh, S., and Pavone, M., "Reduced Order Model Predictive Control For Setpoint Tracking," *European Control Conference*, 2019.

[20] Lorenzetti, J., and Pavone, M., "Error Bounds for Reduced Order Model Predictive Control," , 2019. Available at `http://arxiv.org/abs/1911.12349`.

[21] Lesoinne, M., Sarkis, M., Hetmaniuk, U., and Farhat, C., "A linearized method for the frequency analysis of three-dimensional fluid/structure interaction problems in all flow regimes," *Computer Methods in Applied Mechanics and Engineering*, Vol. 190, No. 24, 2001, pp. 3121–3146.

[22] Wang, Y., and Boyd, S., "Fast model predictive control using online optimization," *IEEE Transactions on Control Systems Technology*, Vol. 18, No. 2, 2010, pp. 267–278.

[23] Regan, C., "mAEWing2: Conceptual Design and System Test," *AIAA Atmospheric Flight Mechanics Conference*, 2017.

[24] McClellan, A., Lorenzetti, J., Pavone, M., and Farhat, C., "Projection-based Model Order Reduction for Flight Dynamics and Model Predictive Control," *AIAA Scitech Forum*, 2020.